CrossMark

Tuning of dielectric and impedance properties of PVDF by incorporation of Mg doped PZT

S. K. Pradhan[1] · Amit Kumar[2] · P. Kour[3] · Rabichandra Pandey[4] · Pawan Kumar[5] · Manoranjan Kar[4] · A. N. Sinha[2]

Abstract

Ferroelectric polymer nanocomposites of poly(vinylidene fluoride) (PVDF) and Mg doped PZT (PMZT) have been prepared by solvent casting method. The existence of β, γ and δ polar phases and α nonpolar phase of PVDF have been observed from the X-ray diffraction (XRD) and FTIR analysis. Both rhombohedral as well as tetragonal crystal phases of PZT at morphotropic phase boundary (MPB) is also observed. The characteristic peaks of PVDF in the FTIR spectra are unaffected with the incorporation of PMZT. Dielectric properties were studied as a function of frequency and temperature. The microstructure of PVDF–PMZT composite has been studied by employing SEM technique. Maximum dielectric constant of 32 with minimum dielectric loss of 0.0053 were obtained at 100 kHz for 6 mol% PMZT composite. The *ac* conductivity follows the Jonscher power law which exhibits the least value of interaction between mobile ions and lattice. Both grain and grain boundary contributions have been considered to explain the impedance behavior of the sample. The optimum loading percentage of PMZT in PVDF matrix is found to be 6 mol%. The structural results obtained from XRD and FTIR are well correlated with the physical parameters obtained from impedance measurement.

1 Introduction

Flexible electronic devices such as sensor, actuator, wearable antenna etc need materials having good electrical and mechanical properties [1]. Ferroelectric polymer nanocomposites can be used in these devices. Ferroelectric polymers with good mechanical and ferroelectric properties are potential materials for making devices [1, 2]. So, these devices are generally mechanical sensors (sensor in the wings of airplanes and sensors used in hydrostatic) and underwater devices, etc. Among the ferroelectric polymers, poly(vinylidene fluoride) (PVDF) is the most promising because of suitable physical properties for technological applications. Its ferroelectric property and high strength makes it suitable for making mechanical sensor. PVDF contains both amorphous and crystalline structures, hence it is semicrystalline in nature. The α, β, γ and δ are the polymorph structures in the crystalline PVDF [3–5]. The polar and non polar phases of this polymer mostly influence its physical properties. The electrical properties of PVDF can be modified for technological needs by making composites with different suitable ceramics. The ferroelectric ceramics have been incorporated in PVDF matrix to enhance its electrical properties significantly for the technological applications. The resulting light weight PVDF–ceramic composite has good mechanical and electrical properties [6–8]. Among the ferroelectric ceramic fillers, lead zirconate titanate (PZT) is the most promising one. It is a solid solution of antiferroelectric lead zirconate ($PbZrO_3$) and ferroelectric lead titanate ($PbTiO_3$) [9]. This ceramic undergoes a structural change with respect to temperature and composition. The composition with Zr/Ti ~ 52/48 exhibits promising dielectric, ferroelectric and piezoelectric property below the Curie temperature [10–12]. PZT at a particular composition (Zr/Ti ~ 52/48) exhibits good electrical properties [13–15]. Doped PZT shows promising electrical properties [16, 17].

✉ S. K. Pradhan
sudiptabitpatna@gmail.com

1 Department of Mechanical Engineering, BIT Mesra, Patna Campus, Patna 800014, India

2 Department of Mechanical Engineering, National Institute of Technology, Patna, Patna 800005, India

3 Department of Applied Physics, BIT Mesra, Patna Campus, Patna 800014, India

4 Department of Physics, Indian Institute of Technology, Patna, Patna 801103, India

5 Department of Physics, Mahatma Gandhi Central University, Motihari, Bihar 845401, India

Isovalent doping in PZT ceramic modify its electrical properties [18, 19].

For mechanical energy harvesting the dielectric electroactive polymer exhibits promising performance. Maximum Electrical properties were obtained at 50 mol% of PZT in PVDF–PZT composite [20]. Modification in the processing of PVDF–PZT composite shows uniform dispersion [21]. Maximum Electrical and mechanical properties of PVDF–PZT composite was obtained for 20 mol% of PZT in the PVDF–PZT composite [22]. For mechanical energy harvesting the dielectric electroactive polymer shows better performance [23]. Various filler are used to enhanced the dielectric properties of PVDF composite [24–28].

Mg doping at the lead site enhances the electrical properties of PZT. Maximum ferroelectric properties have been observed for 10 mol% Mg doped PZT [29]. Hence, PMZT can be a better ferroelectric ceramic as a ceramic filler in PVDF matrix compare to that of PZT. Hence, a nanocomposite of PVDF–PMZT has been prepared and its electrical properties has been explored in this article.

The composite can be prepared with various types of connectivity such as 0–3, 1–3, 2–2 etc. The properties of composites can be used for specific requirements depending on volume fraction, connectivity and properties of fillers. The 0–3 connectivity is easy to prepare compare to other connectivities and it exhibits similar properties in all directions [30–32]. In this 0–3 type ceramic–ploymer composite, isolated ceramic particle is three-dimensionally connected with the polymer matrix. Hence, the composite $(1 − x)$ PVDF-(x) PMZT has been prepared in 0–3 connectivity with x = 2–12% of PMZT.

The literature survey reveals that the physical properties of PVDF–PZT composite can be tuned by controlling the thermal processing conditions [33]. Incorporation of PZT in PVDF matrix leads an enhancement of the electrical properties of PVDF [34–36]. Piezoelectric effect and dielectric constant increase with the increase of PLZT in PLZT–PVDF composites [37].

However, it is expected that the use of Mg substituted PZT as a filler in PVDF matrix will increase the polar β phase in PVDF and hence the electrical polarization will increase. Hence, the objective of the present study is to understand the influence of $Pb_{0.90}Mg_{0.10}ZrTiO_3$ filler in the PVDF matrix. Details crystal structure and electrical properties have been explored.

2 Experimental techniques

PMZT was prepared by the sol–gel method. Lead(II) acetate trihydrate, zirconium(IV) isopropoxide, titanium(IV) isopropoxide, magnesium acetate, 2-methoxyethanol, acetyl acetone and nitric acid of Sigma Aldrich, USA were used as the precursor materials to prepare PMZT. PMZT solution was heated at 100 °C to get the gel of PMZT and gel was dried at 200 °C. The dried powder was calcined at 700 °C for 3 h to get the yellowish PMZT powder. PMZT pellet were prepared and sintered at 1100 °C. The sintered pellets were crushed and used to prepare the composite. Solvent casting method was used to prepare the PVDF–$(Pb(Mg_{0.10}Zr_{0.52}Ti_{0.48})O_3)$ PMZT composite. Dimethyl formamide (DMF) was used to dissolve the PVDF (Sigma Aldrich, USA). In this solution, PMZT powder was added. The solution was sonicated for 50 min at 40 °C until the PVDF and PMZT are well dispersed in DMF. It was then stirred for 6 h at 50 °C and the prepared solution was cast in petri dish and heated at 100 °C for 24 h to get the desired film. X-ray diffraction (XRD) method (Rigaku X-ray diffractometer Model TTRX III in thin film configuration) was employed for the structural analysis of the samples. Here, Cu-Kα radiation with wave length $\lambda = 1.54052$ Å was used. At the room temperature, the XRD data were collected with a scan rate of 2°/min for 2θ in 20°–70° range. Scanning electron microscopy (SEM) was used to study the micrograph of the composite film. Fourier transform infrared spectroscopy (FT-IR) spectra were recorded by the Perkin Elmer (model 400), UK spectrometer in 350–1200 cm^{-1} wave number range. Temperature and frequency dependent dielectric and impedance properties of the sample was measured using N4L LCR meter (PSM1735 Numeric Q), UK attached with a high temperature programmable furnace. The impedance, capacitance in parallel and dielectric loss tangent were measured in between 40 and 120 °C as a function of frequency from 10^2 to 10^6 Hz.

2.1 XRD analysis

X-ray powder diffraction patterns of $(1 − x)$ PVDF-(x) PMZT with x = 0.00–0.12 mol% are shown in the Fig. 1. These observed peaks of the PMZT in the sample matches with ICDD data base (pdf No JSPDS No. 01-070-4060 and b01-073-2022). XRD pattern of $Pb(Mg_{0.10}Zr_{0.52}Ti_{0.48})O_3$ exhibits peaks correspond to both rhombohedral and tetragonal crystal symmetries. The peaks at 22° and 58° correspond to rhombohedral structure [18] where as, the peaks at 30.5°, 37.7°, 43.9° and 54.4° correspond to tetragonal structure of PMZT [18]. Figure 2 shows the enlarged version of measure XRD peak for both rhombohedral and tetragonal crystal symmetries. The XRD pattern of PMZT has been analyzed by employeeing the Rietveld refinement technique by considering both the crystal symmetries. Figure 3 shows the two crystal phases Rietveld analysis of $Pb(Mg_{0.10}Zr_{0.52}Ti_{0.48})O_3$. XRD patterns of PMZT was well refined by considering both R_{3m} and p_{4mm} space groups with Chi^2 $(\chi)^2$ ~ 1.49. It is interesting to note that the crystal symmetry of PMZT does not change in the matrix of PVDF as the peaks are distinctly can be distinguished for
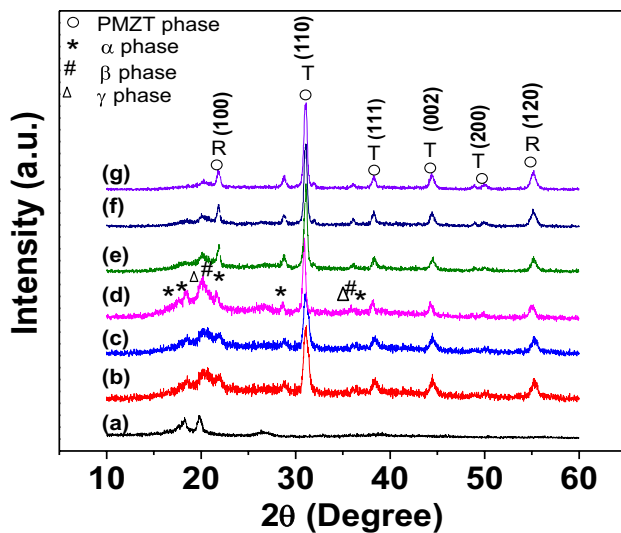
Fig. 1 XRD of (1−x) PVDF-(x) PMZT, (*a*) x=0 mol%, (*b*) x=2 mol%, (*c*) x=4 mol%, (*d*) x=6 mol%, (*e*) x=8 mol%, (*f*) x=10 mol% and (*g*) x=12 mol%

all the composites (shown in Fig. 1). So, the major chemical reaction between PMZT and PVDF is ruled out. Scherrer's formula was used to calculate the crystallite size and, it is found to be ~ 32 nm. The peaks at $2\theta = 18.68°$ and $26.49°$ corresponds to (020) and (021) respectively are the reflection planes of the monoclinic α-phase of PVDF [38–42]. The broad peak at 20.3° corresponds to the crystalline β phase of PVDF with 110/200 reflection plane of orthorhombic structure [39, 42, 43]. The existence of the polar γ phase exhibits the peak at 20.04° which is corresponds to (110) crystalline plane [44]. The polar β phase was increases with the increase in PMZT concentration in the sample. The ratio of β polar phases to nonpolar α has been calculated from the XRD shown in Fig. 8. The concentration of β phase was maximum for 6 mol% of PMZT in the composite. The highest intensity peak for rhombohedral and tetragonal structure of PMZT [18] is shown in
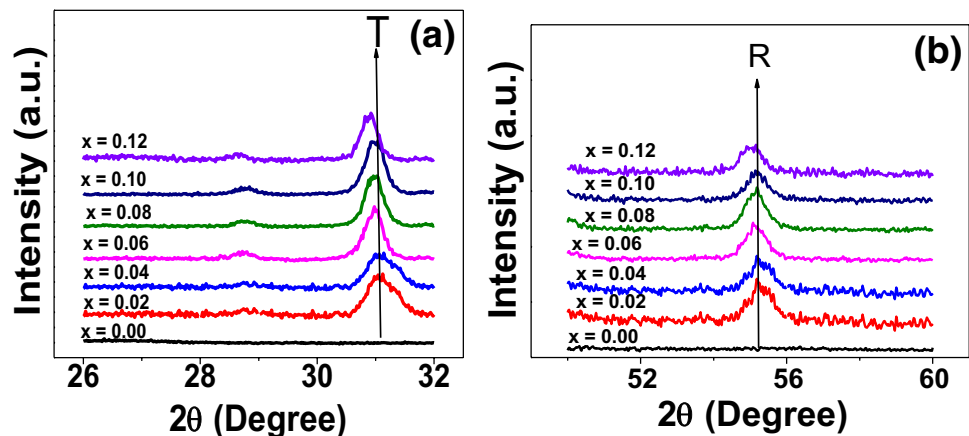
the Fig. 2. It is observed that the peak position for both the structure decreases up to 6 mol% and increases with the further increase in PMZT mol% in the PVDF–PMZT composite. The lattice parameters calculated for PMZT by least square method are enlisted in Table 1 for all the composites. It shows that the lattice parameter increases up to 6 mol% and then decreases. So, 6 mol% composition of PMZT in the composite shows the maximum lattice distortion. Williamson–Hall plot method has been used to calculate the lattice strain of the composite due to incorporation of PMZT in PVDF–PMZT composite. The Williamson–Hall equation defined as [45, 46];

$$\beta \cos\theta = 4\varepsilon \sin\theta + K\lambda/D \tag{1}$$

where β is the fullwidth at half maximum calculated from XRD, ε is the lattice strain, K is the constant usually taken 1 and λ is the wave length of X-ray and D is the crystallite size. The slope of plot between $\beta\cos\theta$ and $\sin\theta$ gives lattice strain and the crystallite size can be calculated from the intercept. Williamson–Hall plot of (1 − x) PVDF-(x) PMZT with x = 0.02–0.12 mol% is shown in Fig. 4a. The lattice strain calculated by using the above equation has been plotted with respect to mol% in Fig. 4b. The lattice strain increases with increase in mol% of PMZT in the composite. It is interesting to note that the strain is maximum for 6 mol%. The shift in symmetric and asymmetric CH$_2$ stretching vibrations (FTIR) due to interfacial interaction between PMZT and PVDF results in the crystallization of the β-phase. Hence maximum stretching can be obtained in 6 mol% of PMZT in the composite which is discussed in Sect. 2.2. Hence, this percentage is identified as the threshold value of PMZT nanofiller in the PVDF matrix for the enhancement of its dielectric and impedance properties.

The scanning electron micrographs of (1 − x) PVDF-(x) PMZT with x = 2, 6 and 12 mol% are shown in the Fig. 5a–c. It is observed that the micrographs are uniform. Hence, it is assumed that the ceramic filler is uniformly distributed in the PVDF matrix.

Fig. 2 Rhombohedral and tetragonal peak in the XRD pattern of (1−x) PVDF-(x) PMZT, x=0 mol%, x=2 mol%, x=4 mol%, x=6 mol%, x=8 mol%, x=10 mol% and x=12 mol%

Fig. 3 Retivelt pattern of $Pb_{0.90}Mg_{0.10}Zr_{0.52}Ti_{0.48}O_3$ sample
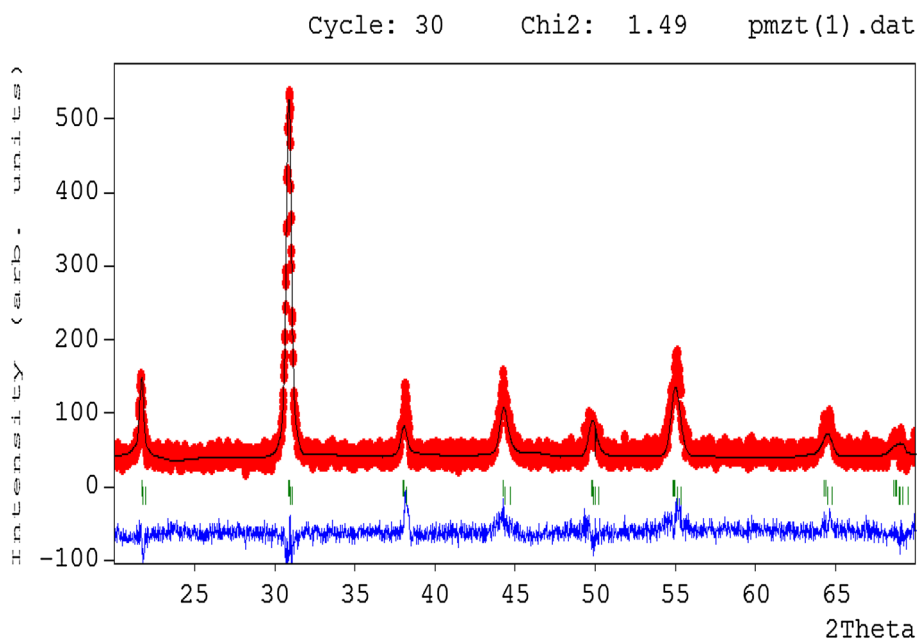
Table 1 Lattice parameters (*a, b, c*) of the $Pb_{1-x}Mg_xZr_{0.52}Ti_{0.48}O_3$ for x = 0.02, 0.04, 0.06 and 0.1 in PVDF–PMZT composite

$Pb_{1-x}Mg_xZr_{0.52}Ti_{0.48}O_3$	Rhombohedral	Tetragonal	
	$a=b=c$ (nm)	$a=b$ (nm)	c (nm)
x = 0.00	0.4158 (± 0.002)	0.4020 (± 0.002)	0.4107 (± 0.002)
x = 0.02	0.4353 (± 0.002)	0.4566 (± 0.002)	0.4093 (± 0.002)
x = 0.04	0.4360 (± 0.002)	0.4680 (± 0.002)	0.4180 (± 0.002)
x = 0.06	0.4481 (± 0.002)	0.4768 (± 0.002)	0.4264 (± 0.002)
x = 0.08	0.4289 (± 0.002)	0.4696 (± 0.002)	0.4132 (± 0.002)
x = 0.10	0.4245 (± 0.002)	0.4668 (± 0.002)	0.4102 (± 0.002)
x = 0.12	0.4066 (± 0.002)	0.46598 (± 0.002)	0.4099 (± 0.002)

Errors are given in bracket

2.2 FTIR spectra analysis

Different types of bond vibrations are associated with the polar and non polar phases of the PVDF and the crystalline phase of PMZT. FT-IR technique is used to study these bond vibrations. FTIR spectra of pure PVDF and different mol% of PMZT in the composite is shown in the Fig. 6. The observed spectrum can be well matched with the PVDF polymer (α and β phases). The absorbance bands at 740,761, 798 and 985 cm^{-1} (Fig. 6) are corresponds to the α-phase of PVDF. The band at 1234 cm^{-1} is assigned to CH$_2$ bending vibration bands. The absorption band at 760 cm^{-1} can be identified as rocking vibration in the PVDF chain. The absorbance bands at 839,872,1076,1155 and 1234 cm^{-1} are correspond to β-phase of PVDF [47–49]. The polar γ phase bands are observed at 778 and 813 cm^{-1}. The bands for polar β and γ phases of the PVDF become stronger where as α phase of the PVDF become

weaker with the increase in mol% of PMZT in the composite. So, the polarity of the composite has been affected by PMZT concentration in the sample. Figure 8 shows the fractions of β phase which is calculated by using Gregorio and Cestari [50] equation:

$$F(\beta) = \frac{A_\beta}{1.2A_\alpha + A_\beta} \tag{2}$$

where A_α and A_β are the absorption band intensities for α and β phases respectively. Fraction of β phase increases with the increase in PMZT concentration in the sample, but exhibits a maximum value for 6 mol%. The β phase decreases with the further increase in PMZT concentration in the sample. Hence, the characteristic of PVDF has changed with the addition of PMZT. The above studies (XRD and FTIR) suggests that the 6% PMZT filler in PVDF is the optimum composition.
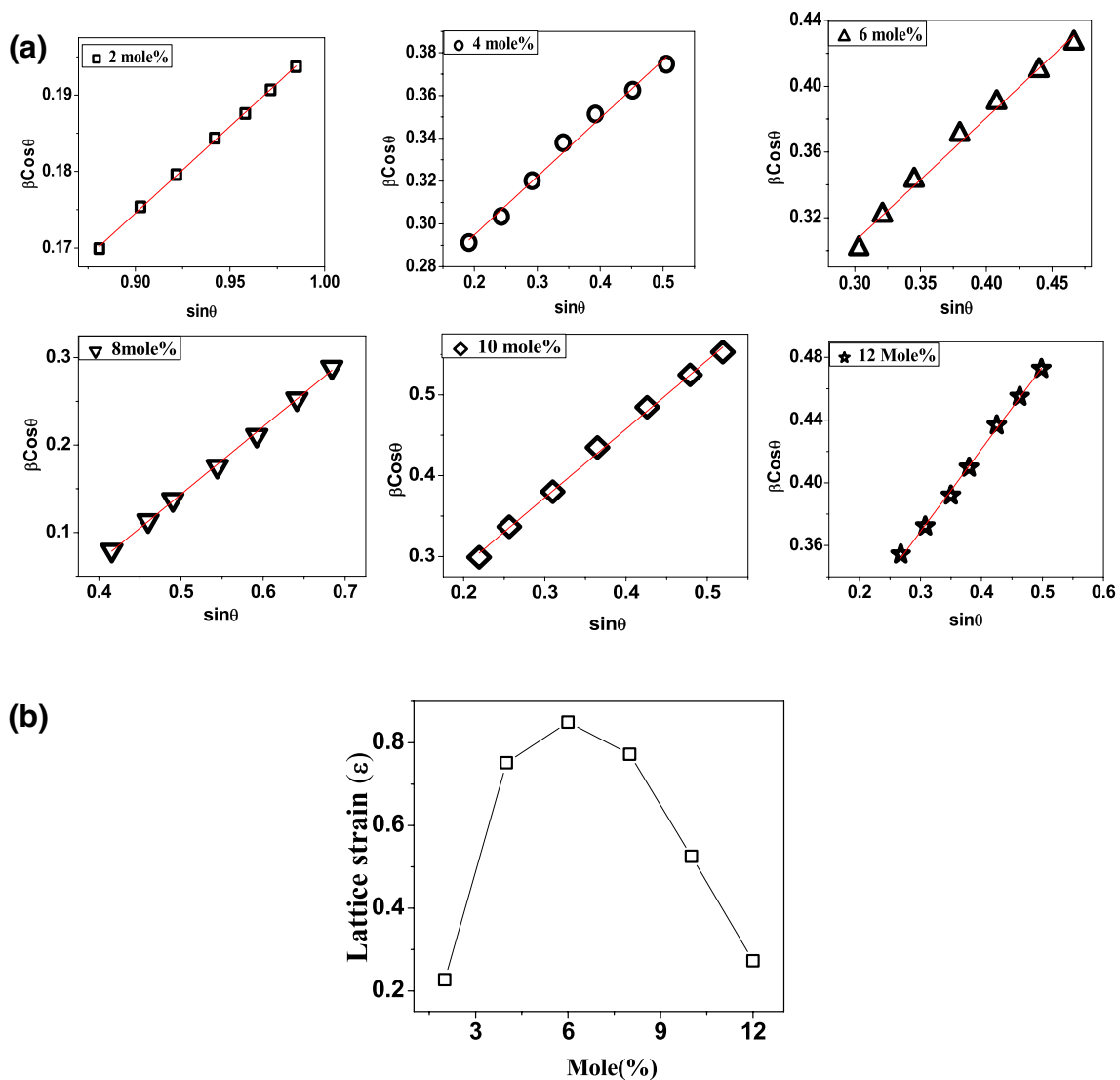
Fig. 4 **a** Williamson–Hall Plot of $(1-x)$ PVDF-(x) PMZT, $x = 2$–12 mol% and **b** Variation of lattice strain with mol% of $(1-x)$ PVDF-(x) PMZT, $x = 2$–12 mol%

2.3 Dielectric properties of PVDF–PMZT composite

Dielectric constant versus temperature plots of $(1-x)$ PVDF-(x) PMZT with $x = 0$–12 mol% are shown in Fig. 7. Dielectric constant of PVDF–PMZT composite almost constant over the temperature range of 40–120 °C. Hence, it is assumed that imperfections/disorders are not created in the lattice with increase in temperature. This may be the interfacial interaction of PMZT in PVDF matrix. So the orientation polarization which is temperature dependent is not comes into play [51]. This result suggests that this composite can be used for a wide high temperature range for technological applications. The dielectric constant increases with the addition of PMZT into the PVDF matrix. However, it is almost constant for 6–12 mol% of

PMZT. Figure 8 shows the variation of dielectric constant and β phase with the increase in PMZT composition in the composite. β phase of PVDF increases with the increase in PMZT composition in the composite. Maximum β phase of PVDF is obtained for 6 mol% of PMZT. Hence, it is assumed that the increase of dielectric constant is due to increase of β phase of PVDF as well as the polarization developed at the interface between PMZT and PVDF, which is mostly can be achieved by ≤ 6 mol% of PMZT in the PVDF matrix. The decrease of dielectric constant for 12 mol% of PMZT could be due to reduction of PVDF chain as well as agglomeration of PMZT, which may have happened due to the large amount of PMZT in the PVDF matrix. Interfacial interaction of PMZT in PVDF increases with increase in mol% of PMZT. Maximum

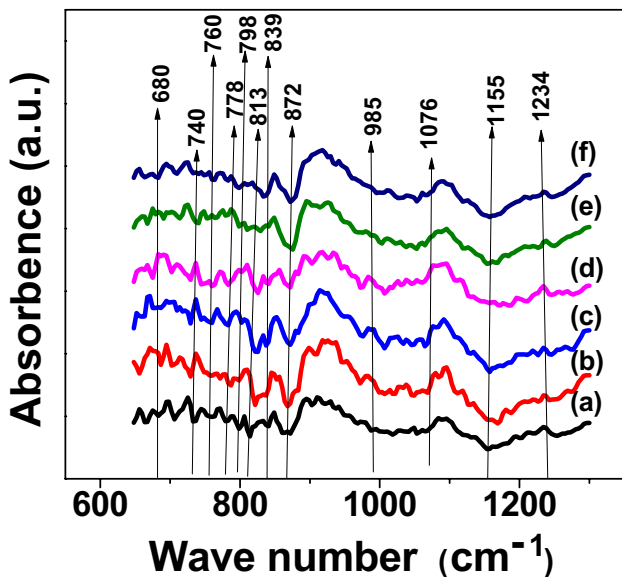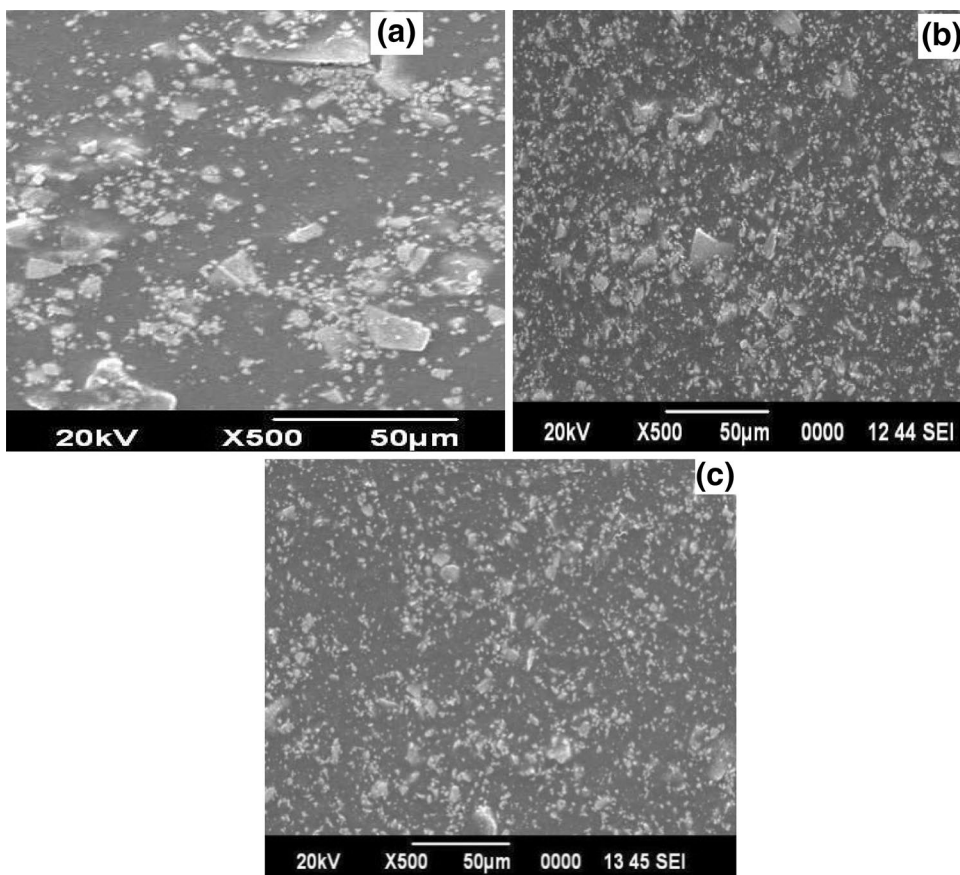**Fig. 5** SEM micrographs of (1 − x) PVDF-(x) PMZT, **a** x = 2 mol%, **b** x = 6 mol and **c** x = 12 mol%

Fig. 6 FTIR of PVDF–Mg doped PZT i.e. (1 − x) PVDF-(x) PMZT, (*a*) x = 2 mol%, (*b*) x = 4 mol%, (*c*) x = 6 mol%, (*d*) x = 8 mol%, (*e*) x = 10 mol% and (*f*) x = 12 mol%

Fig. 7 Variation of dielectric constant with temperature of PVDF–Mg doped PZT i.e. (1 − x) PVDF-(x) PMZT for x = 0 mol%, x = 2 mol%, x = 4 mol%, x = 6 mol%, x = 8 mol%, x = 10 mol% and x = 12 mol%

interaction was obtained for 6 mol% of PMZT supported by FTIR and then the shifting of CH_2 peak decreases resulting decrease in phase in the composite.
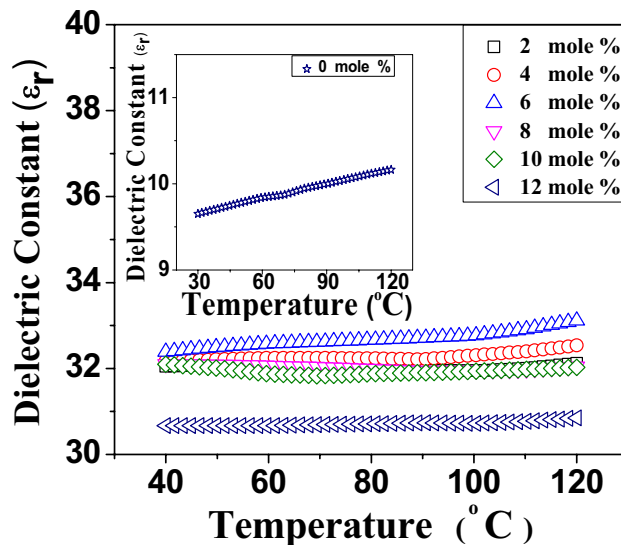
Dielectric constant versus frequency plots for (1 − x) PVDF-(x) PMZT composite (x = 0–12 mol%) are shown in the Fig. 9. It exhibits the usual dielectric behaviour of
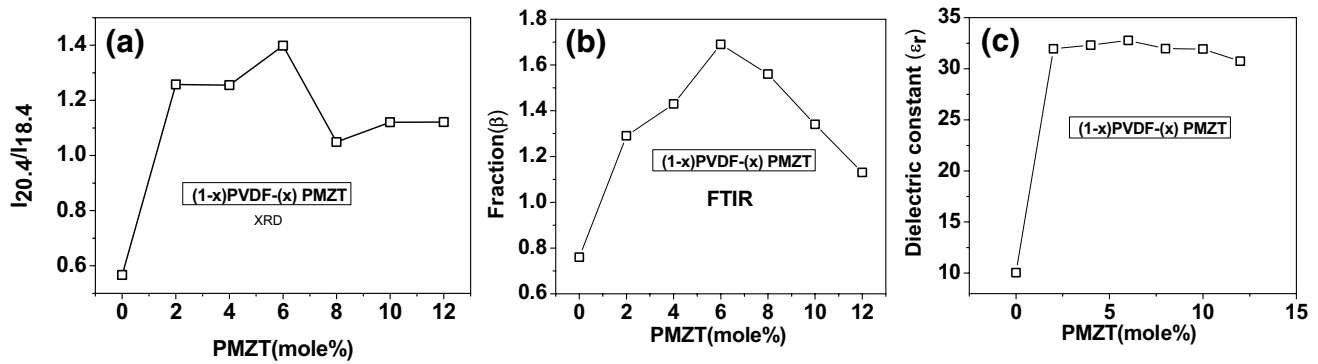
Fig. 8 The β phase of nanocomposites with increasing PMZT obtained from **a** XRD, **b** FTIR analysis and **c** variation of dielectric constants with the increase of PMZT in nanocomposite
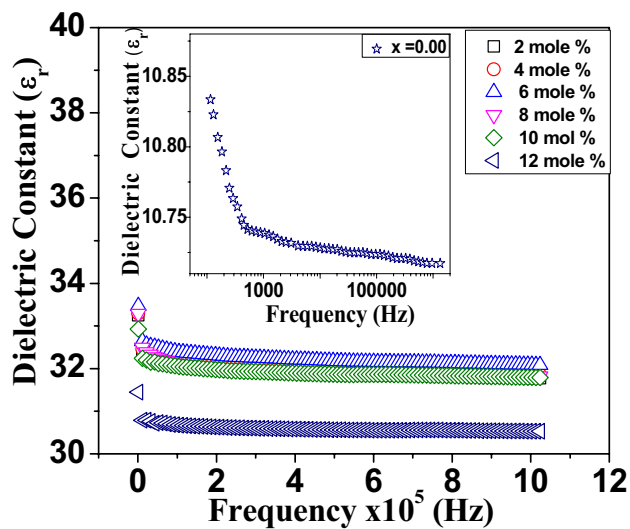

Fig. 9 Variation of dielectric constant with frequency of PVDF–Mg doped PZT i.e. $(1-x)$ PVDF-(x) PMZT, x=0 mol%, x=2 mol%, x=4 mol%, x=6 mol%, x=8 mol%, x=10 mol% and x=12 mol%

Fig. 10 Variation of dielectric loss with frequency of $(1-x)$ PVDF-(x) PMZT composite

a ferroelectric material [52]. The dielectric constant has a maximum value at the lowest frequency and then decreases with the increase in the frequency of the sample. At low frequency, all types of polarisations (ionic, electronic, dipole and space charges polarization) contributes to the dielectric constant. At higher frequencies, the easy depolarization of dipoles that exist at weak bonded interface and boundary regions results in small value of dielectric constant. At higher frequency, only orientational polarization contributes to the dielectric constant. The dielectric constant almost remain constant above 100 kHz. Maximum dielectric constant of 32 was obtained at 100 kHz for 6 mol% of PMZT (Fig. 8). The PMZT incorporation in the PVDF matrix increases the dielectric constant. So, with this high dielectric constant and nearly frequency
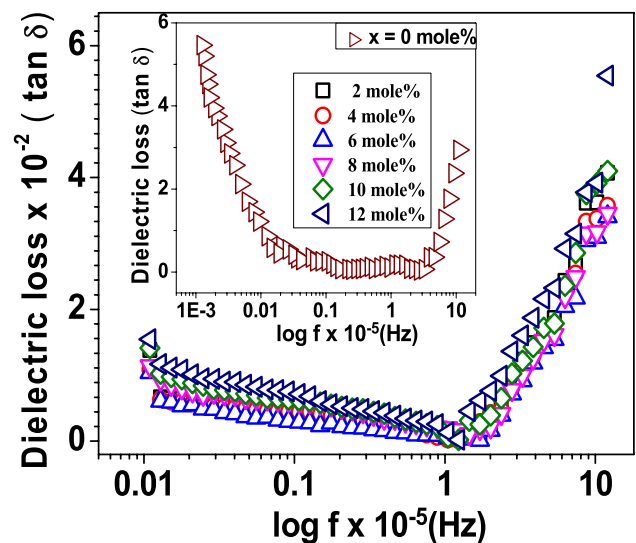
independent nature at high frequency opens a new window for its technological applications.

Variation of dielectric loss with frequency of $(1-x)$ PVDF-(x) PMZT composite is shown in Fig. 10. Dielectric loss decreases with the increase in frequency and, has the lowest value around at 100 kHz. The interfacial dipoles cannot orient themselves in the direction of the alternating field with the increase in frequency. So charges can no longer follow the field and their contribution to the dielectric constant deceases [53]. At high frequency, the dielectric loss increases with the increase in frequency. The dielectric loss decreases with increase in PMZT concentration in the composite and has least value for 6 mol% of PMZT in the PVDF matrix. Dielectric loss increases with further increase in PMZT beyond 6% concentration in the composite.

2.4 Ac conductivity of PVDF–PMZT composite

Plots of Frequency dependent ac conductivity of $(1-x)$ PVDF-(x) PMZT with x = 0–12 mol% are shown in the Fig. 11. The ac conductivity is calculated by using the formula [54] given below;

$$\sigma_{ac} = \omega \varepsilon_r \tan \delta \qquad (3)$$

where ω $(= 2\pi f)$ is the angular frequency, $\tan\delta$ (loss) is the dissipation factor, ε_0 is the free space permittivity and ε_r is the relative permittivity. The curve shows a plateau at lower frequency and, the conductivity increases with the increase in frequency. The conductivity remains nearly constant at high frequency. The ac conductivity decreases with the increase in PMZT composition and has least value for 12 mol% of PMZT composition. The ac conductivity increases with the increase in PMZT concentration in the sample. Maximum ac conductivity was obtained for 6 mol%. Then, ac conductivity decreases with increase in PMZT concentration in the composite. Please give the composite reference/s The similar results were reported on alkaline (Sr) doped PZT ceramics [55]. If the mol% of ceramics increases in the PVDF matrix, it leads to heterogeneous distribution and results in decrease in ac conductivity of the sample. So ac conductivity for > 6 mol% in the PVDF–PMZT decreases. The frequency dependent conductivity is analyzed by employing the Jonscher's power law. It is defined as [56, 57];

$$\sigma_{ac} = \sigma_{dc} + A\omega^n \qquad (4)$$

In the above equation, the temperature dependent pre-exponential factor is A and n is the power law exponent. The plateau in the low frequency region is σ_{dc}. n is varying in

between 0 and 1 and, it is temperature dependent. It represents the measure of interaction between the movable ions with the lattices just about them. Similar results have been obtained by the other groups. $n = 1$ represents that the interaction between adjacent dipoles is almost negligible [58]. The value of A and n are enlisted in the Table 2. The value of A and n are smallest for 6 mol% of PMZT in PVDF matrix and, highest for 12 mol% PMZT in the composite. It is consistent with the dielectric and XRD analysis.

2.5 Impedance analysis of PVDF–PMZT composite

The variation of the real part of impedance (Z′) with frequency plots for $(1-x)$ PVDF-(x) PMZT composite with x = 0–12 mol% are shown in the Fig. 12. Z′ decrease with the increase in frequency and almost constant above 100 kHz frequency. Z′ decreases with the increase in mol% upto 6 mol% of PMZT in PVDF matrix and increase with the

Table 2 A and n values of $(1-x)$ PVDF-(x) PMZT composite for x = 0.00–0.12

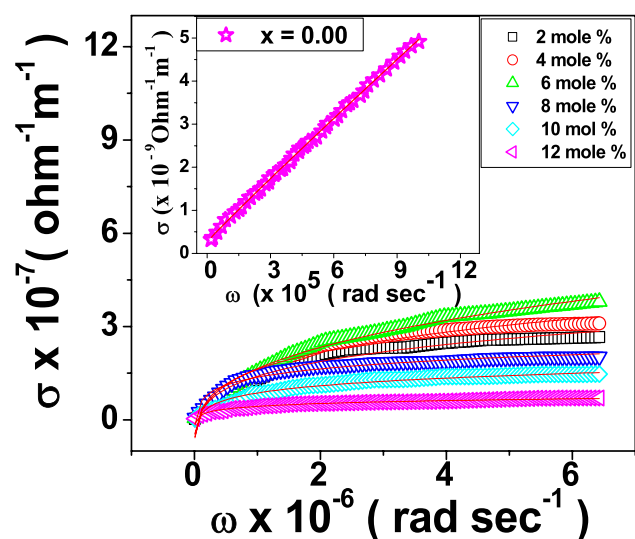| Composition $(1-x)$ PVDF-(x) PMZT	A (S m^{-1} rad^{-n})	n
0.00	7.97E−15	0.96159
0.02	2.20E−08	0.34388
0.04	1.45E−07	0.22539
0.06	1.22E−06	0.21347
0.08	1.55E−07	0.4897
0.10	3.69E−07	0.59479
0.12	8.76E−07	0.9731

Fig. 11 Frequency dependent ac conductivity of $(1-x)$ PVDF-(x) PMZT composite
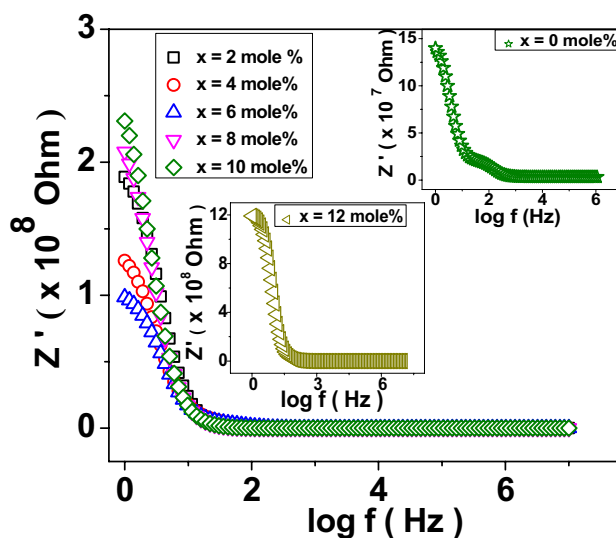

Fig. 12 Variation of Z′ (real) with frequency of $(1-x)$ PVDF-(x) PMZT composite, x = 0–12 mol%

further increase of PMZT mol%. So, the 6 mol% PMZT in PVDF matrix is found to be the optimized percentage. It is consistent with the XRD and dielectric results. So, it is conclude that the bulk resistance is minimum for 6 mol%. And, it was responsible for the observed enrichment of *ac* conductivity of the sample with frequency. Similar results have been observed by other groups [59–62].

The imaginary part of the impedance Z″ represent energy stored in the sample. It depends on the frequency. Frequency dependent Z″ plots for $(1-x)$ PVDF-(x) PMZT composite $(x = 0–12$ mol%) are shown in Fig. 13. Z″ increases with the increase in frequency and shows a peak around 50 kHz and then decreases. It is almost constant for the frequencies greater than 100 Hz. It indicates the possible release of space charges [63]. The asymmetric curves suggest the non-Debye type of relaxation.

The complex impedance analysis gives information about the grain, grain boundary and interface properties such as relaxation frequency, grain and grain boundary resistance, grain and grain boundary capacitance and electronic conductivity. With two consecutive semicircles obtained in Cole–Cole plot gives the contribution from grain and grain boundaries. So, the Cole–Cole technique is used to study the electrical behaviour of the sample [59].

Cole–Cole diagrams of Z′ and Z″ for $(1-x)$ PVDF-(x) PMZT composite are shown in the Fig. 14. The curves are not fully semicircle instead of slightly depression angle. The figure represents two semi-circular arcs. One small semicircle at higher frequency represents the grain property of the sample [60]. The parallel combination of grain capacitance (C_b) and resistance (R_b) represents this property. Another big arc at lower frequency represents grain
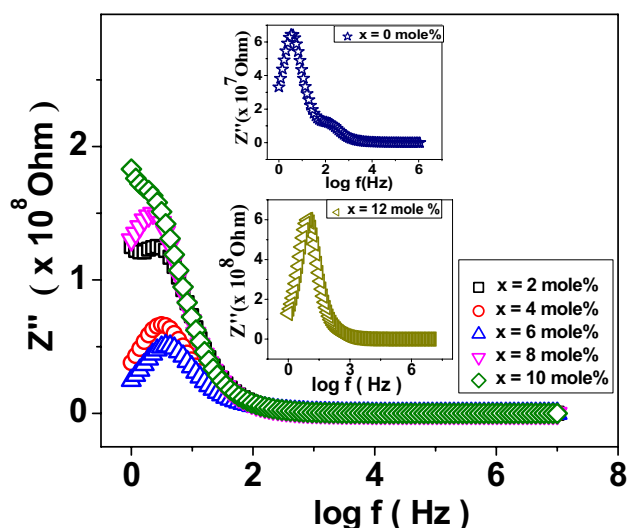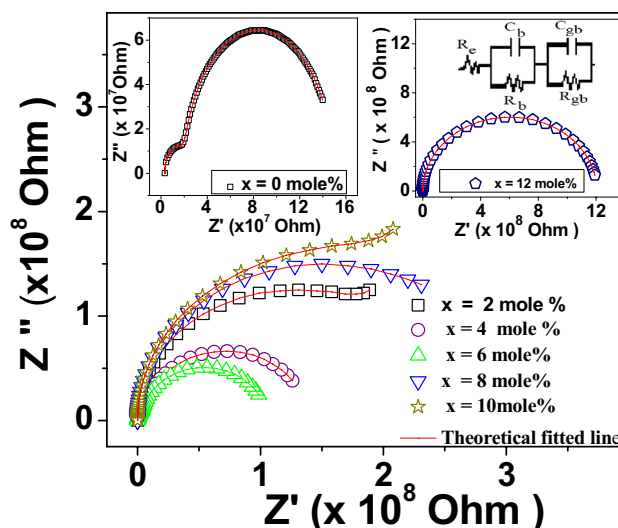

Fig. 14 Cole–Cole plot of $(1-x)$ PVDF-(x) PMZT composite

boundary resistance. This contributes to the grain boundary capacitance (C_{gb}) and resistance (R_{gb}).

ZSimpWin software was used to analyze the data points to the combination of various electronic circuits. Among various electronic circuits $R_e(R_gC_g)(R_{gb}C_{gb})$ could be modelled to the data points with minimum error. Electrode resistance, resistance due to the grain, the resistance due to the grain boundary, capacitance due to grain and capacitance due to grain boundaries were represented by R_e, R_g, R_{gb}, C_g and C_{gb} respectively and these values are enlisted in the Table 3. The grain boundary resistance and grain resistance was least for 6 mol% and highest for 12 mol% PMZT in composite. With increase in PMZT mol% in the composite, the agglomeration of the ceramics results in the increase in grain and grain boundary resistances.

Fig. 13 Variation of Z″ (imaginary) with frequency of $(1-x)$ PVDF-(x) PMZT composite x = 0–12 mol%

Table 3 R_e, R_g and R_{gb} of $(1-x)$ PVDF-(x) PMZT composite

Composition $(1-x)$ PVDF-(x) PMZT	R_e (Ω)	R_g (Ω)	R_{gb} (Ω)
0.00	1.00E−11	3.83E−17	1.93E−17
0.02	1.00E−08	6.57E−16	6.26E−14
0.04	1.42E−07	7.93E−08	2.33E−08
0.06	1.00E−5	2.34E−08	1.32E−05
0.08	1.23E−05	7.93E−08	1.93E−06
0.10	1.00E−6	4.94E−09	9.43E−10
0.12	1.00E−07	1.53E−16	1.64E−16

3 Conclusions

$(1 - x)$ PVDF-(x) PMZT composite ($x = 0, 2, 4, 6, 8, 10$ and 12 mol%) was prepared by the solvent casting method. The presence of both PMZT and PVDF crystal phases were observed in the composite. Hence, there is absence of mesure chemical reaction between PMZT and PVDF phase. The polar β and γ phases increase with the increase in PMZT concentration in the PVDF matrix upto 6 mol% and, decrease with the further increase in PMZT percentage. The dielectric constant increases with the increase in mol% of PMZT in the PVDF–PMZT composite upto 6% and decreases with the further increase. Hence, it is concluded that the composition up to 6 mol% of PMZT enhances the dielectric constant and decrease the conductivity. The dielectric constant is almost constant over the temperature range 40–120 °C. Hence, the present composite is a very good candidate for high temperature application. Also, the impedance remains almost constant for the frequency above 100 kHz, so, it can be used at higher frequency. The optimum mol% of PMZT loading in the PVDF matrix is 6% for enhancing the dielectric properties.

References

1. M. Mai, S. Ke, P. Lin, X. Zeng, J. Nanomater. **16**(1), 181 (2015)
2. Q. Li, Q. Wang, Macromol. Chem. Phys. **217**, 1228 (2016)
3. A.J. Lovinger, Macromolecules **14**, 322 (1981)
4. J.B. Lando, H.G. Olf, A. Peterlin, J. Polym. Sci. A **4**, 941 (1966)
5. J. Lovinger, in *Developments in Crystalline Polymers*, ed. by D.C. Basset (Applied Science Publishers Ltd, Englewood, 1982)
6. Z. Ye, *Handbook of Advanced Dielectric, Piezoelectric and Ferroelectric Materials, Synthesis, Properties and Applications* (CRC Press, Boca Raton, 2008)
7. R. Guo, L.E. Cross, S.E. Park, B. Noheda, D.E. Cox, G. Shirane, Phys. Rev. Lett. **84**(23), 5423 (2000)
8. A.G. Khachaturyan, Phil. Mag. **90**(1–4), 37 (2010)
9. M.E. Lines, A.M. Glass, *Principle and Application of Ferroelectrics and Related Materials* (Clarendon Press, Oxford, 1977)
10. R.E. Newnham, Electroceram. Rep. Prog. Phys. **52**, 123 (1989)
11. G.H. Haerting, Ferroelectric ceramic: history and technology. J. Am. Ceram. Soc. **54**, 1 (1971)
12. B. Jaffe, R.S. Roth, S. Marzullo, J. Res. Natl. Bur. Stan. **55**(5), 239 (1955)
13. B. Jaffe, W.R. Cook, H. Jaffe, *Piezoelectric Ceramics* (Academic Press, London, 1971)
14. D.V. Taylor, D. Damjanovic, Appl. Phys. Lett. **76**(12), 1615 (2000)
15. B. Noheda, L. Wu, Y. Zhu, Phys. Rev. B **66**(6), 060103 (2002)
16. W.L. Warren, G.E. Pike, K. Vanheusden, D. Dimos, B.A. Tuttle, J. Robertson, J. Appl. Phys. **79**(12), 9250 (1996)
17. R.A. Eichel, P. Erhart, P. Träskelin, K. Albe, H. Kungl, M.J. Hoffmann, Phys. Rev. Lett. **100**(9), 095504 (2008)
18. P. Kour, P. Kumar, S.K. Sinha, M. Kar, Solid State Commun. **190**, 33 (2014)
19. P. Kour, P. Kumar, M. Kar, S.K. Sinha, in *AIP Conference Proceedings*, vol. 1536 (2013), p. 667
20. A.K. Biswal, S. Das, A. Roy, in *IOP Conference Series: Materials Science and Engineering*, vol. 178 (2017), p. 012002
21. A. Matei, V. Ţucureanu, P. Vlăzan, I. Cernica, M. Popescu, C. Romaniţan, in *AIP Conference Proceedings*, vol. 1916 (2017), p. 030006
22. J.S. Yun, C.K. Park, Y.H. Jeong, J.H. Cho, J.H. Paik, S.H. Yoon, K.R. Hwang, Nanomater. Nanotechnol. **6**, 20 (2016)
23. A. Kumar, S.F. Ali, A. Arockiarajan, Energy harvesting from crystalline and conductive polymer composites, in *Smart Polymer Nanocomposites* (Springer, Cham, pp 43–75)
24. Q. Guo, Q. Xue, T. Wu, X. Pan, J. Zhang, X. Li, L. Zhu, Compos. A **87**, 46 (2016)
25. X.L. Xu, C.J. Yang, J.H. Yang, T. Huang, N. Zhang, Y. Wang, Z.W. Zhou, Compos. B **109**, 91 (2017)
26. C. Zhang, Q. Chi, J. Dong, Y. Cui, X. Wang, L. Liu, Q. Lei, Sci. Rep. **6**, 33508 (2016)
27. Y. Li, X. Ge, L. Wang, L. Wang, W. Liu, H. Li, Y. Kwok, R. Li, S. Chin, Tjon, Curr. Nanosci. **9**(5), 679 (2013)
28. R. Li, Z. Zhao, C. Zixuan, P. Jianzhong, Mater. Express **7**(6), 536 (2017)
29. P. Kour, P. Kumar, M. Kar, S.K. Sinha, in *AIP Conference Proceedings*, vol. 1512 (2013), p. 1276
30. Y.J. Choi, M.J. Yoo, H.W. Kang, H.G. Lee, S.H. Han, S. Nahm, J. Electroceram. **30**, 30 (2013)
31. L. Zhang, P. Bass, Z.-Y. Cheng, J. Adv. Dielectrics **5**, 1550012 (2015)
32. A.K. Zak, W.C. Gan, W.A. Majid, M. Darroudi, T.S. Velayutham, Ceram. Int. **37**(5), 1653 (2011)
33. V. Tiwari, G. Srivastava, J. Polym. Res. **21**, 587 (2014)
34. P. Gowdhaman, M.H. Pandya, P.R. Kumar, V. Annamalai, J. Environ. Nanotechnol. **4**, 28 (2015)
35. P. Thongsanitgarn, A. Watcharapasorn, S. Jiansirisomboon, Surf. Rev. Lett. **17**, 1 (2010)
36. S.F. Mendes, C.M. Costa, V. Sencadas, J.S. Nunes, P. Costa, J.R. Gregorio, S.L. Mendes, J. Appl. Phys. A **96**, 899 (2009)
37. P. Han, S. Pang, J. Fan, X. Shen, T. Pan, Sens. Actuators A **204**, 74 (2013)
38. T. Lei, X. Cai, X. Wang, L. Yu, X. Hu, G.L. Zheng, W. Wang, D. Wu, D. Sun, L. Lin, RSC Adv. **3**(47), 24952 (2013)
39. S. Chen, K. Yao, F.E.H. Tay, C.L. Liow, J. Appl. Phys. **102**(10), 104108 (2007)
40. D.M. Esterly, B.J. Love, J. Polym. Sci. B **42**(1), 91 (2004)
41. X. Cai, T. Lei, D. Sun, L. Lin, RSC Adv. **7**(25), 15382 (2017)
42. R. Hasegawa, Y. Takahashi, Y. Chatani, H. Tadokoro, Polym. J. **3**(5), 60 (1972)
43. G.T. Davis, J.E. McKinney, M.G. Broadhurst, S. Roth, J. Appl. Phys. **49**(10), 4998 (1978)
44. P. Martins, A.C. Lopes, S. Lanceros-Mendez, Prog. Polym. Sci. **39**(4), 683 (2014)
45. G.K. Williamson, W.H. Hall, Acta Metall. **1**, 22 (1953)
46. C. Suryanarayana, N. Grant, *X-ray Diffraction: A Practical Approach* (Plenum Press, New York, 1998)
47. L. Yu, P. Cebe, Polymer **50**(9), 2133 (2009)
48. V. Ostaševičius, I. Milašauskaitė, R. Daukševičius, V. Baltrušaitis, V. Grigaliūnas, I. Prosyčevas, Mechanika **86**, 78 (2010)
49. T. Boccaccio, A. Bottino, G. Cpannelli, P. Piaggio, J. Membr. Sci. **210**, 315 (2002)
50. R. Gregorio, M. Cestari, J. Polym. Sci. B **32**, 859 (1994)
51. Z.G. Ye (ed.), *Handbook of Advanced Dielectric, Piezoelectric and Ferroelectric Materials: Synthesis, Properties and Applications* (Elsevier, Amsterdam, 2008)
52. L. Kungumadevi, R. Sathyamoorthy, A. Subbarayan, Solid State Electron. **54**, 58 (2010)

53. A.A.M. Farag, A.M. Mansour, A.H. Ammar, M. Abdel Rafea, A.M. Farid, J. Alloys Compd. **513**, 40 (2012)
54. C.R. Mariappan, G. Govindaraj, S. Vinoth Rathan, G. Vijaya, Prakash, Mater. Sci. Eng. B. **121**, 2 (2005)
55. S. Aftab, D.A. Hall, M.A. Aleem, M. Siddiq, J. Mater. Sci.: Mater. Electron. **24**(3), 979 (2013)
56. A.K. Jonscher, *Dielectric Relaxation in Solids* (Chelsea Dielectric Press, London, 1983)
57. A.K. Jonscher, Phys. Status Solidi (b) **83**(2), 585 (1977)
58. K.L. Ngai, C.T. White, A.K. Jonscher, Nature **277**, 185 (1979)
59. J.G. Fletcher, A.R. West, J.T.S. Irvine, J. Electrochem. Soc. **142**(8), 2650 (1995)
60. K.S. Cole, R.H. Cole, J. Chem. Phys. **9**(4), 341 (1941)
61. J.R. Macdonald, *Impedance Spectroscopy* (Wiley, New York, 2005), pp. 17278–17290
62. A. Kumar, N.M. Kumari, R.S. Katiyar, J. Alloys Compd. **469**, 433 (2009)
63. C. León, A. Rivera, A. Várez, J. Sanz, J. Santamaria, K.L. Ngai, Phys. Rev. Lett. **86**(7), 1279 (2001)